Synthesis and characterization of [7]triangulene

SCHOLARONE™
Manuscripts

COMMUNICATION

Synthesis and characterization of [7]triangulene†

Shantanu Mishra,§[a] Kun Xu,§[b] Kristjan Eimre,[a] Hartmut Komber,[c] Ji Ma,[b] Carlo A. Pignedoli,[a] Roman Fasel,*[ad] Xinliang Feng,*[b] and Pascal Ruffieux*[a]

Triangulene and its π-extended homologues constitute non-Kekulé polyradical frameworks with high-spin ground states, and are anticipated to be key components of organic spintronic devices. We report a combined in-solution and on-surface synthesis of the hitherto largest triangulene homologue, [7]triangulene ($C_{78}H_{24}$), consisting of twenty-eight benzenoid rings fused in a triangular fashion. We employ low-temperature scanning tunneling microscopy to confirm the chemical structure of individual molecules adsorbed on a Cu(111) surface. While neutral [7]triangulene in the gas-phase is predicted to have an open-shell septet ground state; our scanning tunneling spectroscopy measurements, in combination with density functional theory calculations, reveal chemisorption of [7]triangulene on Cu(111) together with considerable charge transfer, resulting in a closed-shell state. Furthermore, substantial hybridization between the molecular orbitals of [7]triangulene is observed.

The family of triangular nanographenes with zigzag periphery, hereafter [n]triangulenes,[1] where $n \geq 2$ denotes the number of zigzag carbon atoms per edge, comprise a homologous series of open-shell polybenzenoid compounds (Fig. 1a). The underlying basis for the open-shell ground states of this family is a sublattice imbalance in the bipartite honeycomb lattice, such that it is impossible to pair all p_z-electrons into π-bonds, thus generating radicals.[2,3] Application of Ovchinnikov's rule[4,5] to [n]triangulenes predicts a high-spin ground state (that is, $S > 0$, where S denotes the ground state total spin quantum number) with a linear scaling of S with n, results that have been independently confirmed with a range of theoretical calculations.[6–10] As a result, [n]triangulenes have been

envisaged as key components of carbon-based electronic and spintronic devices, such as qubits for quantum computation and electrically controllable magnetic switches.[11–13] The synthetic chemistry of [n]triangulenes began with the early attempt of Clar in 1953 to synthesize [3]triangulene (or, triangulene).[14] Since then, derivatives of [2]triangulene (or phenalenyl radical)[15] and triangulene[16–18] have been obtained in solution. However, the open-shell ground states of these compounds render a solution-based synthetic approach difficult, and requires kinetic and/or thermodynamic stabilization of the compounds to confer stability for characterization. In this regard, on-surface synthesis[19] under ultrahigh vacuum offers a promising route to achieve such reactive compounds, and allows atomic-scale structural, electronic and magnetic characterization of individual molecules via scanning probe microscopy techniques. Using this approach, the synthesis of triangulene on Cu(111), NaCl(100) and Xe(111) was reported in 2017,[20] which was swiftly followed by syntheses of [4]-[21] and [5]triangulene[22] on Au(111) and Cu(111) in 2019 (Fig. 1a), and covalent triangulene dimers[23] on Au(111) in 2020. However, synthesis of higher homologues remains elusive, given the increasing polyradical character of [n]triangulenes with increasing size (which could lead to enhanced reactivity for higher homologues) and the challenge of designing appropriate molecular precursors suitable for on-surface synthesis.[24] Here, we report a combined in-solution and on-surface synthesis of the hitherto largest triangulene homologue, [7]triangulene (**7T**), on Cu(111), and its structural and electronic characterization via scanning tunneling microscopy and spectroscopy (STM and STS), in combination with density functional theory (DFT) calculations.

Our synthetic strategy toward **7T** involves design of the molecular precursor 2,2',2''-(5'-(3,5-dimethylphenyl)-3,3'',5,5''-tetramethyl-[1,1':3',1''-terphenyl]-2',4',6'-triyl)tripyrene (**1**, Fig. 1b), where the methyl groups of the 3,5-dimethylphenyl moieties are expected to undergo surface-catalyzed oxidative ring closure against the pyrene moieties to yield **7T**. The synthesis of **1**, together with its isomer **1'**, was peformed

a. *nanotech@surfaces Laboratory, Empa – Swiss Federal Laboratories for Materials Science and Technology, Dübendorf, Switzerland.*
b. *Faculty of Chemistry and Food Chemistry, and Center for Advancing Electronics Dresden, Technical University of Dresden, Dresden, Germany.*
c. *Leibniz Institute of Polymer Research Dresden, Dresden, Germany.*
d. *Department of Chemistry and Biochemistry, University of Bern, Bern, Switzerland.*
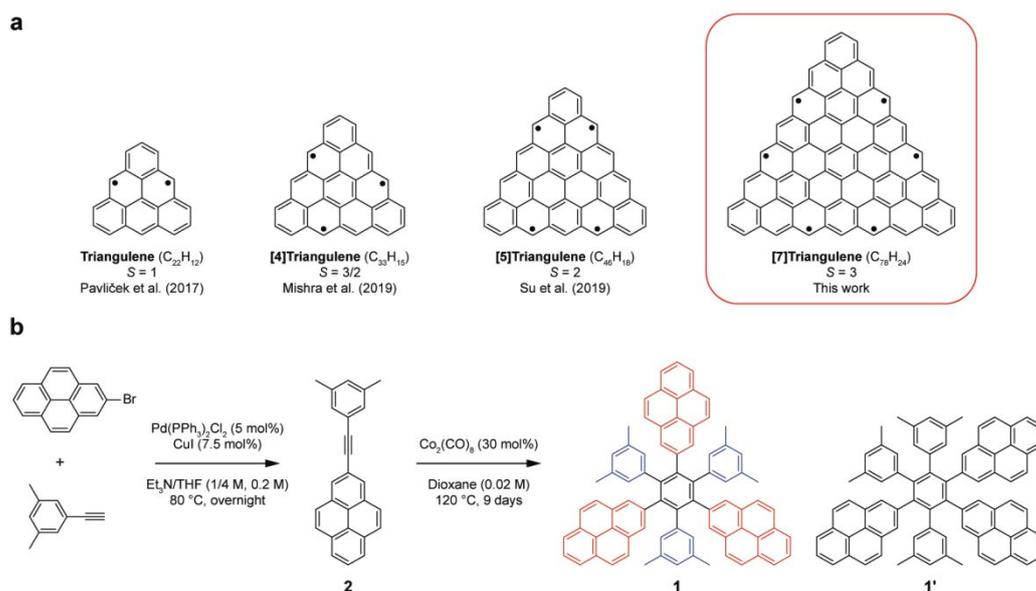
Fig. 1 (a) Series of [*n*]triangulenes that have been synthesized on surfaces. (b) Solution synthesis of precursor **1**.

through cobalt-catalyzed cyclotrimerization of 2-((3,5-dimethylphenyl)ethynyl)pyrene (**2**), which was obtained via Sonogashira coupling of 2-bromopyrene and 1-ethynyl-3,5-dimethylbenzene. The separation to obtain the pure precursor **1** from the solution was unsuccessful despite extensive efforts, and therefore the precursor mixture **1**+**1'** was directly used for subsequent on-surface synthesis.

We first attempted the on-surface synthesis of **1** on Au(111), which is the least active among all coinage metal surfaces, and is shown to only weakly perturb the intrinsic electronic structure of open-shell nanographenes.[25] The presumably extreme reactivity of **7T** precludes the formation of isolated

nanographenes on Au(111), and we only observed covalently coupled molecular clusters (Fig. S1, ESI†). To circumvent this problem, we conducted the on-surface synthesis of **7T** on the more active Cu(111) surface. To this end, a submonolayer coverage of the precursor mixture was sublimed on a Cu(111) surface held at room temperature, and the surface was subsequently annealed to 275 °C to promote the on-surface reactions. Fig. 2a presents the overview STM image of the surface after the annealing step, revealing triangular nanographenes (highlighted with a square), along with rhomboidal nanographenes (highlighted with an arrow) and a minority of partially reacted precursor molecules. Fig. 2b shows
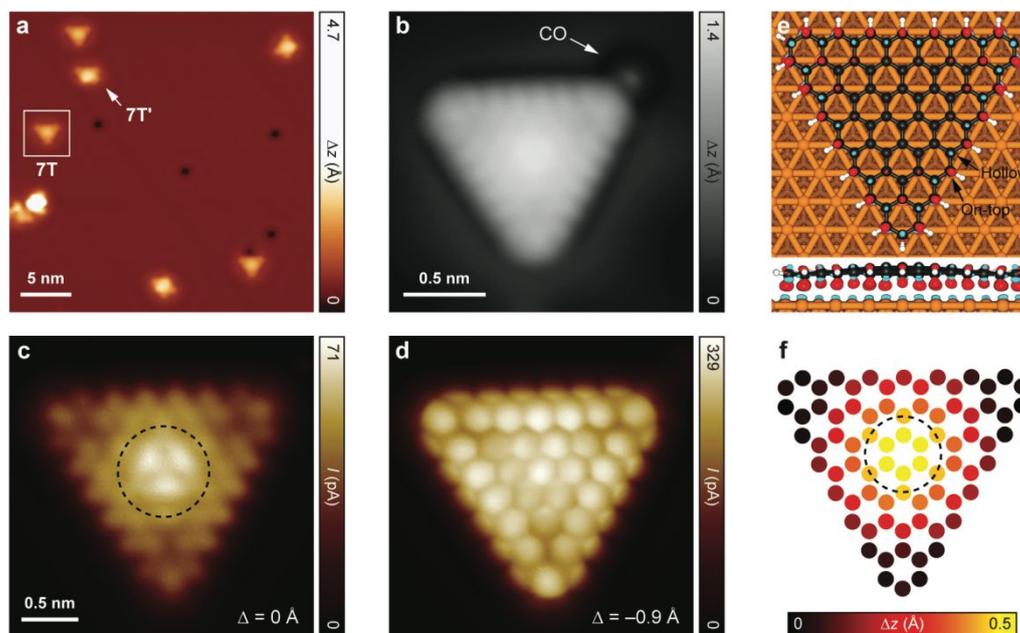
Fig. 2 (a) Overview STM image after annealing precursor mixture **1**+**1'** on Cu(111) at 275 °C ($V = -1.20$ V, $I = 50$ pA). (b) High-resolution STM image of **7T** acquired with a CO functionalized tip ($V = -0.10$ V, $I = 200$ pA). A co-adsorbed CO molecule is indicated. (c and d) Ultrahigh-resolution STM images of **7T** acquired at $\Delta = 0$ Å (c) and -0.9 Å (d) (open feedback parameters: $V = -5$ mV, $I = 50$ pA). (e) Top and side views of the DFT optimized geometry of **7T** on Cu(111), with overlaid DFT charge density difference plot (isovalue: 0.004 a.u.). Red/cyan isosurfaces indicate charge accumulation/depletion. (f) Two-dimensional map of the DFT calculated relative heights of the carbon atoms of **7T** adsorbed on Cu(111). Each filled circle represents a carbon atom.

the high-resolution STM image of a triangular nanographene, which presents a uniform three-fold symmetric appearance consistent with **7T**, and additionally exhibits a noticeable modulation in the local density of states (LDOS) along its three edges. To access the chemical structure of the nanographene, we performed constant-height ultrahigh-resolution STM imaging with a carbon monoxide (CO) functionalized tip in the regime of tip-molecule Pauli repulsion.[26,27] Fig. 2c and d show the ultrahigh-resolution STM images acquired with two different offsets (Δ) applied to the tip-sample distance with respect to the STM set point above the nanographene. Imaging at close tip-sample distances (Δ = −0.9 Å, Fig. 2d) yields the internal bond structure of the nanographene, which corresponds to **7T**, thereby proving the success of our synthetic protocol. On the other hand, imaging at far tip-sample distances (Δ = 0 Å, Fig. 2c) does not provide bond resolution, but reveals a notable non-uniformity in the distribution of the tunneling current over **7T**, with the current being the highest at the center of **7T** (highlighted with a dashed circle) and the lowest at the vertices. To unveil the origin of this observation, we performed DFT structural analysis of the **7T**/Cu(111) system. Fig. 2e presents the DFT-optimized geometry of **7T** on Cu(111), where it is seen that **7T** adsorbs with its zigzag edges oriented along the nearest neighbor Cu atomic rows, such that all the majority sublattice carbon atoms occupy the on-top Cu sites, while the minority sublattice atoms occupy the three-fold coordinated

hollow sites. Fig. 2f presents a two-dimensional map of the relative heights of the carbon atoms of **7T** adsorbed on Cu(111) from DFT calculations. From this data, it is inferred that **7T** adopts a dome-shaped configuration on Cu(111), with the average height difference between the carbon atoms of the central hexagonal ring (highlighted with a dashed circle) and the hexagonal rings at the vertices being ~ 0.5 Å (the adsorption heights of the lowest and highest carbon atoms of **7T** with respect to the top Cu layer are ~ 2.4 and 2.9 Å, respectively). Therefore, during constant-height scanning, the central region of **7T**, which is the closest to the tip, registers the maximum tunneling current (see Fig. S2, ESI† for a series of ultrahigh-resolution STM images of **7T**). Additionally, STM analysis of the rhomboidal nanographene highlighted in Fig. 2a shows that it corresponds to the product obtained from cyclodehydrogenation and oxidative cyclization reactions of **1'** (**7T'**; see Fig. S3, ESI†).

Charge density difference calculations of **7T**/Cu(111) (Fig. 2e) reveal substantial charge redistribution within the system, with considerable accumulation of electrons at the peripheral zigzag carbon atoms of **7T** and electron depletion from the Cu atoms directly underneath, indicating chemisorption of **7T** on Cu(111). To quantify the charge transfer in the system, we performed Bader charge analysis[28,29] on the DFT charge density of the **7T**/Cu(111) system, which reveals a charge transfer of 2.32 electrons from Cu(111) to **7T**, resulting from the interplay
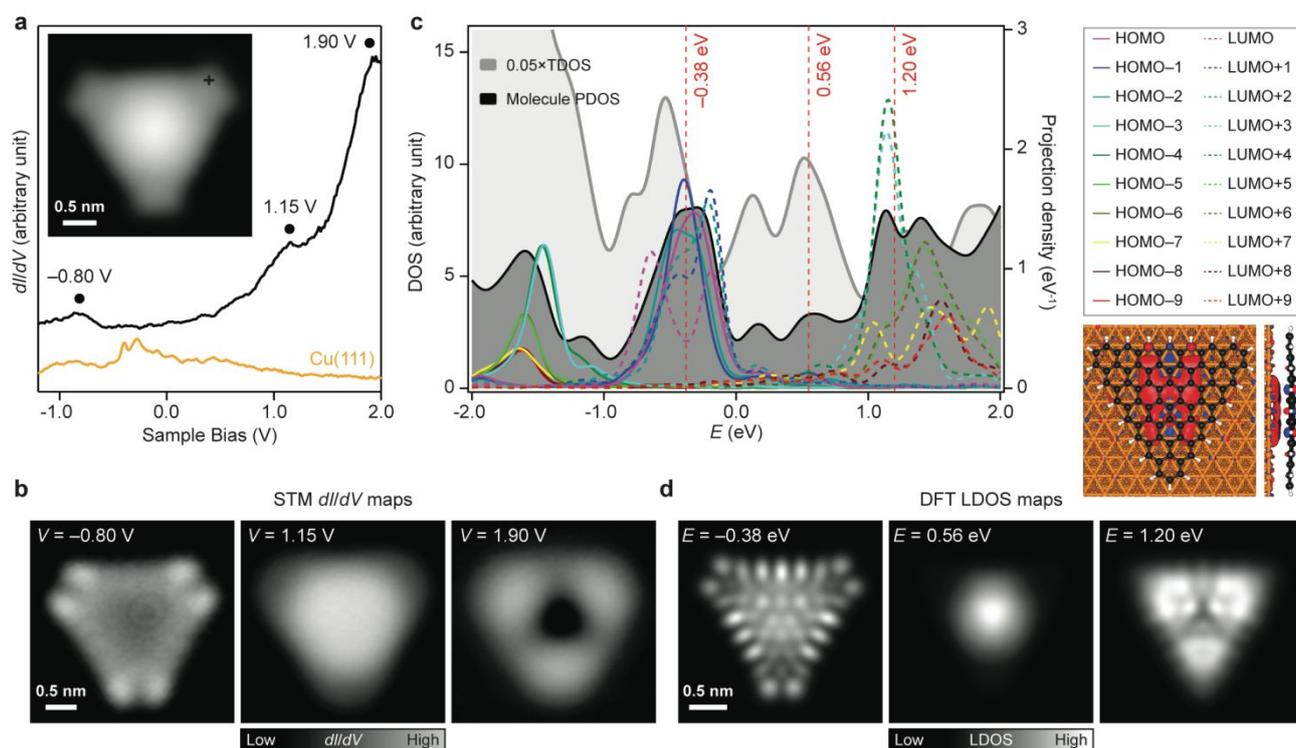
Fig. 3 (a) dI/dV spectrum acquired on **7T** (black curve) at the position indicated in the inset STM image (open feedback parameters: V = −1.20 V, I = 350 pA; V_{rms} = 14 mV). Scanning parameters for the STM image: V = −0.80 V, I = 330 pA. (b) Constant-current dI/dV maps acquired at the resonances indicated in (a) (I = 330–350 pA; V_{rms} = 22 mV). (c) PDOS (solid black curve, left ordinate) on **7T** for the **7T**/Cu(111) system, and projection of the orbitals of gas-phase **7T** to the orbitals of the **7T**/Cu(111) system (solid and dashed colored curves, right ordinate), along with the TDOS (solid grey curve, left ordinate) of the **7T**/Cu(111) system scaled by a factor of 0.05. A Gaussian broadening with a full width at half maximum of 0.20 eV has been applied to all curves. Abscissa indicates energy with respect to the Fermi energy of Cu(111). Also shown at the bottom right is the orbital isosurface of one of the representative orbitals of the **7T**/Cu(111) system contributing to the LDOS map at 0.56 eV (isovalue: 0.01 a.u.). (d) DFT simulated LDOS maps at the energies indicated by the vertical dashed lines in (c), calculated at a height of 4 Å above the molecular plane.

of orbital energy alignment and C-Cu bond formations. We studied the magnetic ground state of **7T** in the gas phase and on Cu(111) through spin-polarized DFT calculations. While **7T** was found to exhibit an open-shell septet (S = 3) ground state in the gas phase (in accordance with Ovchinnikov's rule), with the open-shell quintet (S = 2), triplet (S = 1), singlet (S = 0) and closed-shell states 0.25, 0.30, 0.33 and 1.29 eV higher in energy, respectively (Fig. S4, ESI†), it was found to be closed-shell on Cu(111).

We studied the experimental electronic structure of **7T** on Cu(111) via STS. *dI/dV* spectroscopy (where I and V correspond to the tunneling current and voltage, respectively), which provides a measure of LDOS beneath the STM tip, on **7T** reveals a broad peak at −0.80 V along with two shoulders at 1.15 V and 1.90 V (Fig. 3a). Fig. 3b presents the corresponding spatially resolved *dI/dV* maps at these bias voltages. The resonance at −0.80 V has maximum intensity along the edges of **7T**, similar to the spin-polarized edge states previously found for [n]triangulenes (n = 3–5). The resonance at 1.15 V appears as a featureless circular area of high intensity at the central region of **7T**, with weaker intensities at the vertices. Finally, the resonance at 1.90 V appears as three lobes at the vertices of **7T**, along with a node at the center. To uncover the origin of these states, we performed a DFT projected density of states (PDOS) analysis of the **7T**/Cu(111) system (Fig. 3c), where the projection analysis was performed on the closed-shell gas phase molecular orbitals (MOs) of **7T**. Our results show that the gas phase frontier orbitals of **7T** (that is, the six orbitals labeled HOMO−2 to LUMO+2) hybridize into a single DOS peak below the Fermi energy at ~ −0.38 eV, while at ~ −1.50 eV, we observe the hybridization of the gas phase HOMO−3 and HOMO−4, with minor contribution from low-lying orbitals. Above the Fermi energy, we observe a strong DOS peak at ~ 1.20 eV with main contribution from the hybridization of the gas phase LUMO+3 and LUMO+4, and minor contribution from high-lying orbitals. DFT LDOS maps at −0.38 eV and 1.20 eV (Fig. 3d) exhibit good match with the *dI/dV* maps at −0.80 V and 1.90 V, respectively, indicating that the state at −0.80 V corresponds to the hybridized HOMO−2 to LUMO+2, while the state at 1.90 V predominantly corresponds to the hybridized LUMO+3 and LUMO+4. We note that till −2.00 V, we do not experimentally detect the hybridized HOMO−3 and HOMO−4. Furthermore, between the Fermi energy and 1.20 eV in the PDOS plot, we observe a considerable **7T**/Cu(111) total density of states (TDOS) contribution at ~ 0.56 eV. Both from the PDOS plot and the orbital visualization presented in Fig. 3c, it is seen that this state contains negligible contribution from the MOs of **7T**, with the majority contribution coming from the underlying surface. We therefore assign this state to a primarily bound and localized Cu(111) surface state, exhibiting weak admixture with the MOs of **7T**. It is to be noted that the DFT LDOS map at 0.56 eV exhibits excellent agreement with the *dI/dV* map at 1.15 V, which thus completes the electronic characterization of **7T** on Cu(111). Finally, we note that spin polarization of **7T** on Cu(111) would lead to the detection of spin-split singly occupied MOs in STM experiments, which appear similar at both bias polarities, as has been previously observed for [n]triangulenes (n = 3–5).[20–23]

However, we conducted sequential *dI/dV* mapping of **7T** on Cu(111) between −2.00 V and 1.90 V (Fig. S5, ESI†), and found no signatures of singly occupied MOs, which provides an experimental indication of the closed-shell ground state of **7T** on Cu(111).

In conclusion, we have shown the successful synthesis of [7]triangulene on Cu(111), which is the hitherto largest triangulene-based system. Our synthetic protocol combines solution synthesis of precursor **1**, which undergoes oxidative cyclization reactions on Cu(111) surface to yield the final product **7T**. High-resolution STM imaging at submolecular resolution confirms the chemical structure of **7T**, and reveals its non-planar geometry on the surface. STS measurements, in conjunction with DFT calculations, reveal charge transfer between Cu(111) and **7T**, and considerable hybridization of the MOs of **7T**, leading to a closed-shell ground state of **7T** on Cu(111). Our synthetic methodology opens new opportunities in the realization of nanoscale polyradical frameworks, leading to interesting avenues to explore spin interactions and spin lifetimes in all-organic nanostructures by inelastic electron tunneling spectroscopy and STM-based electron spin resonance[30] experiments. However, the strong perturbation of the intrinsic electronic structure of **7T** on metal surfaces necessitates decoupling or transfer of such molecules onto insulators.

Conflicts of interest

There are no conflicts to declare.

Acknowledgements

References

1 Y. Morita, S. Suzuki, K. Sato and T. Takui, *Nat. Chem.,* 2011, **3**, 197–204.
2 W. L. Wang, O. V. Yazyev, S. Meng and E. Kaxiras, *Phys. Rev. Lett.,* 2009, **102**, 157201.

3   Z. Bullard, E. Costa Girão, C. Daniels, B. G. Sumpter and V. Meunier, *Phys. Rev. B*, 2014, **89**, 245425.

4   A. A. Ovchinnikov, *Theoret. Chim. Acta*, 1978, **47**, 297–304.

5   E. H. Lieb, *Phys. Rev. Lett.*, 1989, **62**, 1201–1204.

6   J. Fernández-Rossier and J. J. Palacios, *Phys. Rev. Lett.*, 2007, **99**, 177204.

7   M. Ezawa, *Phys. Rev. B*, 2007, **76**, 245415.

8   W. L. Wang, S. Meng and E. Kaxiras, *Nano Lett.*, 2008, **8**, 241–245.

9   A. Das, T. Müller, F. Plasser and H. Lischka, *J. Phys. Chem. A*, 2016, **120**, 1625–1636.

10 R. Ortiz, R. A. Boto, N. García-Martínez, J. C. Sancho-García, M. Melle-Franco and J. Fernández-Rossier, *Nano Lett.*, 2019, **19**, 5991–5997.

11 A. D. Güçlü, P. Potasz, O. Voznyy, M. Korkusinski and P. Hawrylak, *Phys. Rev. Lett.*, 2009, **103**, 246805.

12 A. D. Güçlü, P. Potasz and P. Hawrylak, *Phys. Rev. B*, 2011, **84**, 035425.

13 W.-L. Ma and S.-S. Li, *Phys. Rev. B*, 2012, **86**, 045449.

14 E. Clar and D. G. Stewart, *J. Am. Chem. Soc.*, 1953, **75**, 2667–2672.

15 K. Goto, T. Kubo, K. Yamamoto, K. Nakasuji, K. Sato, D. Shiomi, T. Takui, M. Kubota, T. Kobayashi, K. Yakusi and J. Ouyang, *J. Am. Chem. Soc.*, 1999, **121**, 1619–1620.

16 G. Allinson, R. J. Bushby, J. L. Paillaud, D. Oduwole and K. Sales, *J. Am. Chem. Soc.*, 1993, **115**, 2062–2064.

17 G. Allinson, R. J. Bushby, M. V. Jesudason, J.-L. Paillaud and N. Taylor, *J. Chem. Soc., Perkin Trans. 2*, 1997, 147–156.

18 J. Inoue, K. Fukui, T. Kubo, S. Nakazawa, K. Sato, D. Shiomi, Y. Morita, K. Yamamoto, T. Takui and K. Nakasuji, *J. Am. Chem. Soc.*, 2001, **123**, 12702–12703.

19 S. Clair and D. G. de Oteyza, *Chem. Rev.*, 2019, **119**, 4717–4776.

20 N. Pavliček, A. Mistry, Z. Majzik, N. Moll, G. Meyer, D. J. Fox and L. Gross, *Nat. Nanotechnol.*, 2017, **12**, 308–311.

21 S. Mishra, D. Beyer, K. Eimre, J. Liu, R. Berger, O. Gröning, C. A. Pignedoli, K. Müllen, R. Fasel, X. Feng and P. Ruffieux, *J. Am. Chem. Soc.*, 2019, **141**, 10621–10625.

22 J. Su, M. Telychko, P. Hu, G. Macam, P. Mutombo, H. Zhang, Y. Bao, F. Cheng, Z.-Q. Huang, Z. Qiu, S. J. R. Tan, H. Lin, P. Jelínek, F.-C. Chuang, J. Wu and J. Lu, *Sci. Adv.*, 2019, **5**, eaav7717.

23 S. Mishra, D. Beyer, K. Eimre, R. Ortiz, J. Fernández-Rossier, R. Berger, O. Gröning, C. A. Pignedoli, R. Fasel, X. Feng and P. Ruffieux, *Angew. Chem. Int. Ed.*, 2020, **59**, 12041–12047.

24 J. Su, M. Telychko, S. Song and J. Lu, *Angew. Chem. Int. Ed.*, 2020, **59**, 7658–7668.

25 S. Mishra, D. Beyer, K. Eimre, S. Kezilebieke, R. Berger, O. Gröning, C. A. Pignedoli, K. Müllen, P. Liljeroth, P. Ruffieux, X. Feng and R. Fasel, *Nat. Nanotechnol.*, 2020, **15**, 22–28.

26 L. Gross, F. Mohn, N. Moll, P. Liljeroth and G. Meyer, *Science*, 2009, **325**, 1110.

27 G. Kichin, C. Weiss, C. Wagner, F. S. Tautz and R. Temirov, *J. Am. Chem. Soc.*, 2011, **133**, 16847–16851.

28 R. F. W. Bader, *Atoms in Molecules: A Quantum Theory*, Oxford University Press, Oxford, 1994.

29 W. Tang, E. Sanville and G. Henkelman, *J. Phys.: Condens. Matter*, 2009, **21**, 084204.

30 S. Baumann, W. Paul, T. Choi, C. P. Lutz, A. Ardavan and A. J. Heinrich, *Science*, 2015, **350**, 417–420.